

Radiationless energy exchange in three-soliton collisions

Sergey V. Dmitriev^{1,*}, Panayotis G. Kevrekidis², and Yuri S. Kivshar³

¹*Institute for Metals Superplasticity Problems RAS, Khalturina 39, 450001 Ufa, Russia*

²*Department of Mathematics and Statistics, University of Massachusetts, Amherst, MA 01003 USA*

³*Nonlinear Physics Center, Research School of Physical Science and Engineering, Australian National University, Canberra, 0200 ACT, Australia*

We revisit the problem of the three-soliton collisions in the weakly perturbed sine-Gordon equation and develop an effective three-particle model allowing to explain many interesting features observed in numerical simulations of the soliton collisions. In particular, we explain why collisions between two kinks and one antikink are observed to be practically elastic or strongly inelastic depending on relative initial positions of the kinks. The fact that the three-soliton collisions become more elastic with an increase in the collision velocity also becomes clear in the framework of the three-particle model. The three-particle model does not involve internal modes of the kinks, but it gives a qualitative description to all the effects observed in the three-soliton collisions, including the fractal scattering and the existence of short-lived three-soliton bound states. The radiationless energy exchange between the colliding solitons in weakly perturbed integrable systems takes place in the vicinity of the separatrix multi-soliton solutions of the corresponding integrable equations, where even small perturbations can result in a considerable change in the collision outcome. This conclusion is illustrated through the use of the reduced three-particle model.

PACS numbers:

I. INTRODUCTION

The study of soliton collisions in nonintegrable systems [1, 2] is interesting because such systems typically describe more realistic situations than the integrable systems where the interactions between solitons are known to be purely elastic [3]. In nonintegrable systems, the collision outcome can be highly nontrivial and, depending on the degree of nonintegrability, the collision scenario can have qualitatively different features.

For the classical ϕ^4 equation,

$$\frac{\partial^2 u}{\partial t^2} - \frac{\partial^2 u}{\partial x^2} + u - u^3 = 0, \quad (1)$$

which is rather far from an integrable system, kink collisions are always accompanied by a certain amount of radiation in the form of small-amplitude wave packets, as well as by the excitation of the kink's internal modes [4]. The latter are responsible for several effects in the ϕ^4 kink-antikink collisions. In particular, the resonant energy exchange between the translational motion of the kinks and their internal modes explains the fractal kink-antikink scattering [5]. This is a topic that was initiated by the numerical studies in Ref. [6] (see also Ref. [7] and references therein), and it is still under active investigation [8].

For long time, the excitation of the soliton internal modes and the radiation losses were thought to be two major manifestations of inelasticity of the soliton collisions in nonintegrable models. However, a qualitatively different manifestation was recently identified, namely,

the radiationless energy exchange (REE) between colliding solitons [9, 10, 11, 12, 13, 14, 15, 16, 17] (abbreviated as "REE" in Ref. [10], a designation that we will use hereafter).

The energy transferred to soliton internal modes in soliton collisions, for small ϵ , is typically proportional to ϵ^2 , and the same is true for the radiation losses (here ϵ is the coefficient in front of a perturbation term, added to an integrable equation). Terms proportional to ϵ^2 appear as the lowest-order correction terms in the collective variable approaches used to describe the soliton's internal modes [4]; the kink dynamics in the discrete ϕ^4 equation [18]; the kink and breather dynamics in the discrete sine-Gordon equation (SGE) [19, 20]; and the radiation from the discrete SGE kink [21] and from the soliton in the discrete nonlinear Schrödinger equation (NLSE) [1]. On the other hand, the degree of inelasticity due to the REE effect, when the latter is present (see details below) grows proportionally to ϵ [10, 11]. This means that for weakly perturbed integrable systems the REE effect becomes a dominant manifestation of the inelasticity of collision, while the soliton's internal modes and radiation become increasingly important with stronger deviations from integrable case.

The REE effect can also be responsible for the fractal soliton scattering which was demonstrated for the first time in [14] for the weakly perturbed SGE and later for the weakly perturbed NLSE [15, 16]. In contrast to those studies, in Refs. [22, 23] the fractal scattering of vector solitons in the coupled NLSE was attributed to the resonance energy exchange between the soliton's translational and internal modes, i.e., through the mechanism similar to that operating for the ϕ^4 kinks [5, 6, 7, 8].

Fractal soliton scattering in the weakly perturbed NLSE was explained qualitatively in the frame of a very

*Electronic address: dmitriev.sergey.v@gmail.com

simple model [15] and for the generalized NLSE in the context of a more elaborate collective variable approach [24], based on the method of Karpman and Solov'ev [25]. Remarkably, the soliton's internal modes were not involved into consideration in [15, 24] indicating that the underlying dominant mechanism for the fractal scattering was the REE effect (rather than the internal mode excitation).

For weakly perturbed integrable systems, parameters of the colliding solitons where the REE effect is observed can be found from the analysis of the corresponding *integrable* equation. This was done for the weakly perturbed SGE in [12] and for the weakly perturbed NLSE in [16] using the fact that the REE effect is observed in the vicinity of separatrix multi-soliton solutions of the integrable equation.

In the case of moderate deviation from integrability, it becomes increasingly important to check if the degree of nonintegrability and the sign of perturbation allows for the existence of noticeable soliton internal modes before one can judge to which extent the REE effect and the soliton internal modes contribute to the inelasticity of collision (see, e.g., Sec. II D in [17]). The effect of the REE effect in the case of a moderate degree of non-integrability has studied far less extensively than in the case of weak perturbation, though valuable results have been recently obtained for the discrete NLSE [26] and for the generalized NLSE with various types of the nonlinear term [24], where a general system of ordinary differential equations was derived for the velocities, amplitudes, positions and phases of the solitary waves. The latter was shown to qualitatively and quantitatively match the predictions of the full model.

In this paper, we study the REE effect in three-soliton collisions of a weakly perturbed sine-Gordon equation. In the frame of the three-particle model, we demonstrate that the REE effect is directly related to a separatrix solution, and it offers a very transparent explanation of the origin of fractal soliton scattering. We also classify in a general way the potential for emergence of such phenomena in three-kink collisions of the weakly perturbed sine-Gordon model.

The paper is organized as follows. In Sec. II, the results of numerical study of the degree of inelasticity of three-soliton collisions in the Frenkel-Kontorova model Eq. (2) are presented. First, the collisions between three kinks/antikinks are analyzed in Sec. II A and then the kink-breather collisions are investigated in Sec. II B. The three-particle model is introduced and analyzed in Sec. III. The discussion of the results and our conclusions are presented in Sec. IV.

II. THREE-SOLITON COLLISIONS IN WEAKLY DISCRETE SGE

To study the effects of non-integrability on the soliton collisions it is desirable to have a model with tunable

deviation from an integrable case [c.f. with Eq. (1) which does not have such a parameter]. The Frenkel-Kontorova (FK) model,

$$\frac{d^2 u_n}{dt^2} - \frac{1}{h^2}(u_{n-1} - 2u_n + u_{n+1}) + \sin u_n = 0, \quad (2)$$

which is a discretization of the integrable SGE,

$$u_{tt} - u_{xx} + \sin u = 0, \quad (3)$$

is a convenient choice for such a study [12, 13, 14]. The (singular) perturbation parameter in Eq. (2) is $\epsilon = h^2$ (with h being the lattice spacing); the lowest order correction to SGE due to the discretization can be quantified, upon a Taylor expansion of the second difference, as $(\epsilon/12)u_{xxxx}$.

The exact three-soliton solutions to SGE are well known [12, 27]. The solutions are the combinations of single-soliton solutions, namely kinks (K) or antikinks (\bar{K}), having the topological charges $q = 1$ and $q = -1$, respectively, and two-soliton solutions, namely breathers (B), which are actually the kink-antikink oscillatory bound states.

Energy E and momentum P of one SGE kink are defined by its velocity V as follows

$$E_K = 8\delta, \quad P_K = 8V\delta, \quad \text{where } \delta^{-1} = \sqrt{1 - V^2}. \quad (4)$$

Energy and momentum of a breather are defined by its frequency ω and velocity V :

$$E_B = 16\eta\xi, \quad P_B = 16\eta\xi V, \\ \text{where } \xi^{-1} = \sqrt{1 - V^2}, \quad \eta = \sqrt{1 - \omega^2}. \quad (5)$$

Below we describe the numerical results for the three-soliton collisions in the weakly discrete ($h^2 = 0.04$) SGE Eq. (2). The exact three-soliton solutions to SGE were employed for setting the initial conditions. The equations of motion Eq. (2) were integrated with the use of the Störmer method of order six. We register the parameters of quasi-particles after their collision and compare them with those before the collision. The larger the change in the parameters, the more inelastic the collision is.

A. Three-kink collisions

We number the kinks in a way that at $t = 0$ (before the collisions) their initial positions are related as $(x_0)_1 < (x_0)_2 < (x_0)_3$ and momenta as $P_{K_1} > P_{K_2} > P_{K_3}$. Here we consider only symmetric collisions with $P_{K_1} > 0$, $P_{K_2} = 0$, and $P_{K_3} = -P_{K_1}$. Consideration of non-symmetric collisions does not bring any new important physical effects. For the symmetric collisions it is convenient to set $(x_0)_1 = -(x_0)_3$ so that the three-soliton collisions are expected when $(x_0)_2$ is close to the origin, otherwise the two successive two-soliton collisions will take place. Thus, among the kink's initial positions $(x_0)_i$ the only essential parameter is $(x_0)_2$.

Finally, our three-kink system is defined by the topological charges of the kinks. There are eight possible variants in assigning the charges to the three kinks, which, due to symmetry, can be divided into three groups of topologically different collisions: $K\bar{K}K = \bar{K}K\bar{K}$, $KKK = \bar{K}\bar{K}\bar{K}$, and $KK\bar{K} = \bar{K}K\bar{K} = K\bar{K}K = \bar{K}K\bar{K}$. We will refer to each group by referring to their first member.

The collision outcome is presented by the momenta of kinks after collision, \tilde{P}_{K_j} , as the functions of $(x_0)_2$ for a given P_{K_1} , which defines the initial momenta of the kinks, P_{K_j} , as described above. In some cases a kink-antikink pair can merge into a breather. In those cases we assumed that the kinks constituting the breather share its momentum equally, in order to plot their momenta.

The results for the KKK collisions are shown in Fig. 1 (a) for $P_{K_1} = 0.8$. Similar results for the $KK\bar{K}$ collisions are shown in Fig. 1 (b) also for $P_{K_1} = 0.8$. The results for the $K\bar{K}K$ collisions are shown in Fig. 2 (a) for $P_{K_1} = 2.5$ (larger collision velocity) and in Fig. 2 (b) for $P_{K_1} = 0.8$ (smaller collision velocity).

In the panels (a') and (b') of Fig. 1 and Fig. 2 the examples of collisions are presented on the (x, t) plane by showing the regions of energy density greater than a certain value, so that the cores of the solitons are clearly seen. These examples are given for the particular values of the initial coordinate of the middle kink, $(x_0)_2$, indicated by the arrows in the corresponding panels at left.

First we note that KKK and $KK\bar{K}$ collisions are always practically elastic regardless of the specifics of $(x_0)_2$ (see Fig. 1) and only $K\bar{K}K$ collisions are inelastic for $(x_0)_2$ close to the origin (see Fig. 2). We conclude that if a kink has positive or negative charge with equal probability, then the REE in three-kink collisions can be expected in two cases from eight.

Of particular importance is the fact that in the strongly inelastic $K\bar{K}K$ collisions shown in Fig. 2 the energy given to the kink's internal modes and to the radiation is negligible in comparison to the energy exchange between the quasi-particles [12]. This is the main feature of REE effect in soliton collisions.

The $K\bar{K}K$ collisions can be strongly inelastic because in this case the cores of all three kinks can merge. Two-kink collisions are practically elastic for the considered case of weak perturbation, $h^2 = 0.04$, as it can be seen in Fig. 1 (b), (b'). To explain why the two-kink collisions are elastic we note that Eq. (2) conserves energy and, for small perturbation parameter h^2 , the momentum is also conserved with a high accuracy while the higher-order conservation laws of SGE are destroyed by the weak discreteness. The conservation of energy and momentum sets two constraints on the two parameters of the two-kink solution. A three-kink solution has one free parameter and REE becomes possible if all three kinks participate in a collision.

For the $K\bar{K}K$ collisions we note that the collision with a larger velocity [see Fig. 2 (a), (a')] results only in quan-

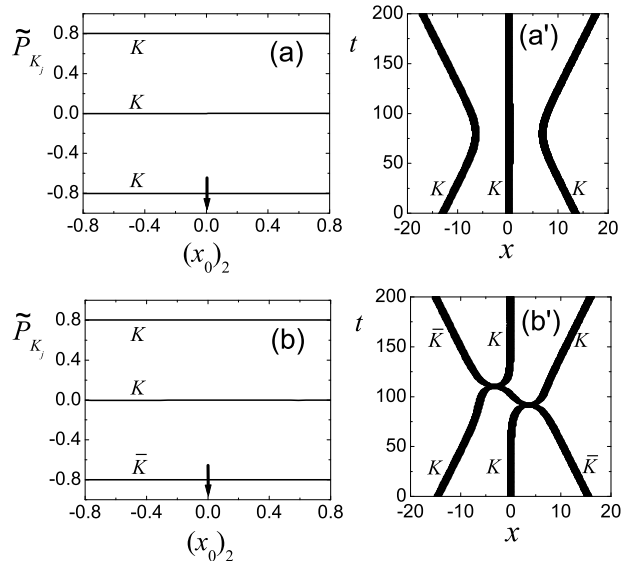


FIG. 1: Numerical results for (a), (a') KKK and (b), (b') $KK\bar{K}$ collisions in FK model. The left panels show the momenta of the kinks after collision \tilde{P}_{K_j} as the functions of the initial position of middle kink, $(x_0)_2$. In both cases momenta of the kinks before the collision were $P_{K_1} = -P_{K_3} = 0.8$ and $P_{K_2} = 0$ and they are nearly same after the collision meaning that the collisions are practically elastic for any $(x_0)_2$. The right panels show the examples of collisions on the (x, t) plane for $(x_0)_2 = 0$ by plotting the regions with the energy density greater than certain value, so that the cores of the solitons are clearly seen.

titative change of kink parameters, while collision with a smaller velocity [see Fig. 2 (b), (b')] may result in fusion of a kink-antikink pair in a breather. The result of $K\bar{K}K$ collisions is extremely sensitive to variations in $(x_0)_2$ in the vicinity of $(x_0)_2 = 0$, especially for small collision velocities.

A simple explanation of the fact that the collisions between two kinks and an antikink are always practically elastic for $KK\bar{K}$ and can be strongly inelastic in the case of $K\bar{K}K$ will be offered in Sec. III.

In the case of weak perturbation we never observed fractal patterns in the three-kink collisions (recall that in the ϕ^4 model such patterns can be observed even in two-kink collisions but, as it was already mentioned, this model is far from an integrable one), while it can be observed in the kink-breather collisions, as discussed below, and in the breather-breather collisions [14].

B. Kink-breather collisions

Without loss of generality, we assume $P_K + P_B = 0$. Then we have two parameters, the momentum P_B and frequency ω of the breather. The outcome of the KB

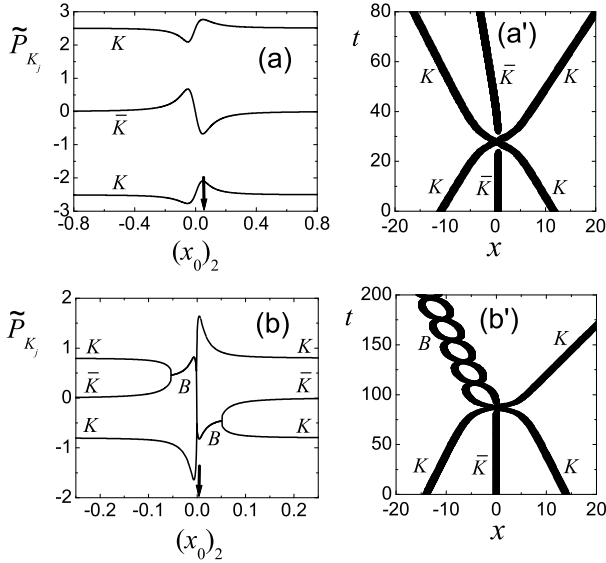


FIG. 2: Numerical results for $K\bar{K}K$ collisions with (a), (a') $P_{K_1} = 2.5$ (larger collision velocity) and (b,b') $P_{K_1} = 0.8$ (smaller collision velocity) in the FK model. The left panels show the momenta of the kinks after collision \tilde{P}_{K_j} as the functions of the initial position of middle kink, $(x_0)_2$. Collisions are strongly inelastic for $(x_0)_2$ close to the origin. The right panels show the examples of collisions on the (x, t) plane for (a') $(x_0)_2 = 0.05$ and (b') $(x_0)_2 = 0.01$ by plotting the regions with the energy density greater than a certain value, so that the cores of the solitons are clearly seen. Collision with a larger velocity in (a), (a') results only in quantitative change of kink parameters while collision with a smaller velocity in (b), (b') may result in fusion of a kink-antikink pair in a breather.

collisions is studied as a function of the initial separation between the kink and the breather controlled by the initial kink position $(x_0)_K$.

In Fig. 3 we plot the momenta of kinks after collision, \tilde{P}_{K_j} (including the kinks constituting the breather, assuming as earlier that they share the breather's momentum equally), as a function of $(x_0)_K$ for (a) $P_B = 2.5$ (larger collision velocity) and (b) $P_B = 1.6$ (smaller collision velocity). One can see that strong REE is possible in the KB collisions. Note that in Fig. 3 only a small part of one period of the output functions is shown for the region with strong REE. In (a) there is a range of $(x_0)_K$ where the breather obtains enough energy to split into a kink-antikink pair [example is shown in (a')]. In (b), in addition to this possibility, there appears a region where the breather is reflected from the kink [example is shown in (b')].

For large collision velocities [somewhat larger than in Fig. 3 (a), (a')] the kink passes through the breather with no qualitative change in the collision outcome; there is only some energy and momentum exchange between

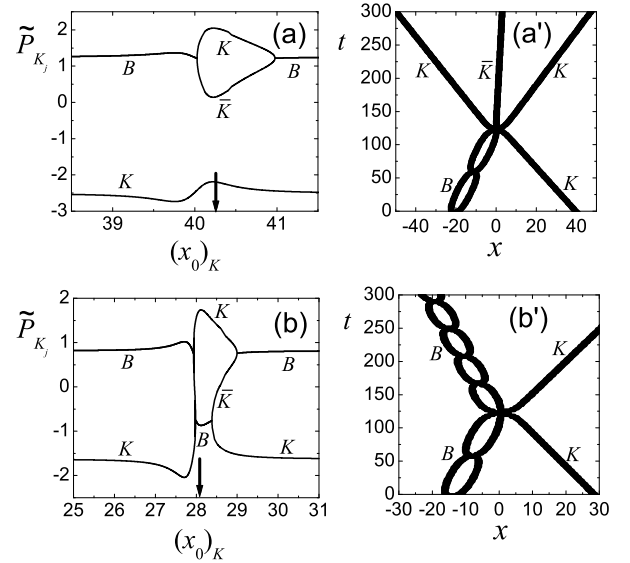


FIG. 3: Numerical results for the kink-breather collisions in FK model for (a), (a') $P_B = 2.5$ (larger collision velocity) and (b,b') $P_B = 1.6$ (smaller collision velocity) and $\omega = 0.05$ in both cases. The left panels show the momenta of the kinks after the collision \tilde{P}_{K_j} as a function of the initial position of the kink, $(x_0)_K$. The right panels show examples of collisions on the (x, t) plane for (a') $(x_0)_K = 40.25$ and (b') $(x_0)_K = 28.1$.

them. However, for sufficiently small collision velocity the collision outcome as the function of the initial separation between the kink and breather is a fractal. An example is presented in Fig. 4 for $\omega = 0.3$, $P_B = 0$ (kink and breather have zero initial velocities), where the soliton's momenta after collision \tilde{P}_{K_j} are shown as the functions of $(x_0)_K$.

The structure presented in Fig. 4 can be described as a chain of self-similar patterns. At each scale smooth regions are separated by the apparently chaotic regions of two symmetry types, one shown in (a) and (d) and another one in (b) and (c). (b) and (d) present blowups of the regions indicated in panel (a); (c) is a blowup of the region indicated in (b).

Two examples of the kink-breather dynamics are given in Fig. 5 for (a) $(x_0)_K = 0.24$ and (b) $(x_0)_K = 0.236$ [indicated in Fig. 4 (b) by the arrows A and B, respectively]. The three-particle solution has a certain lifetime L (in this example $L \approx 55$) and then it splits into a kink and a breather. Similar dynamics has been reported, e.g., for the breather-breather system in the weakly discrete FK model [14], in the weakly perturbed NLSE [15], and recently for the generalized NLSE [24]. Thus, this type of dynamics is rather general. For the two-soliton collisions in the weakly perturbed NLSE we have estimated numerically the probability p to observe the three-particle

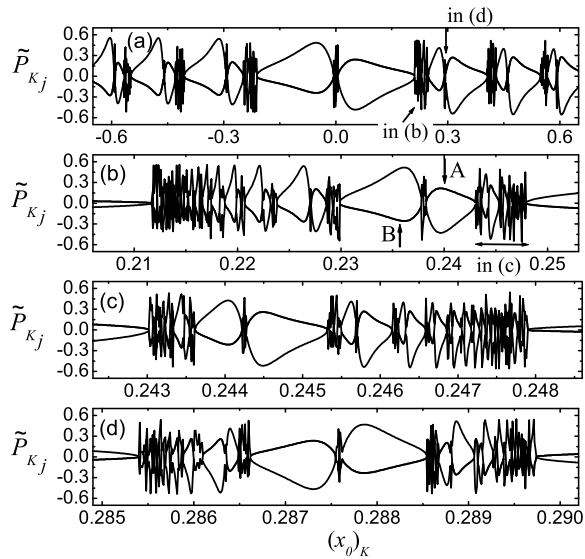


FIG. 4: Fractal kink-breather scattering observed for $\omega = 0.3$, $P_B = 0$ (kink and breather have zero initial velocities). The kinks' momenta after the collision \tilde{P}_{K_j} are shown as the functions of the initial position of the kink, $(x_0)_K$, at different scales. At each scale smooth regions are separated by the apparently chaotic regions of two symmetry types, one shown in (a) and (d) and another one in (b) and (c). (b) and (d) present blowups of the regions indicated in panel (a); (c) is a blowup of the region indicated in (b).

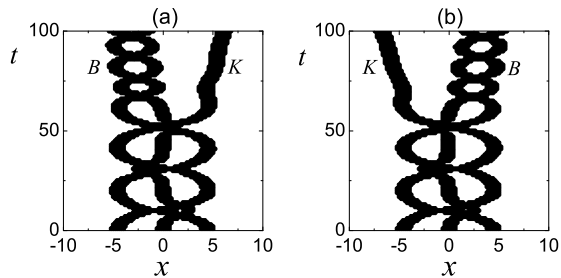


FIG. 5: Examples of the kink-breather dynamics for (a) $(x_0)_K = 0.24$ and (b) $(x_0)_K = 0.236$ [indicated in Fig. 4 (b) by the arrows A and B, respectively].

system with the lifetime L and found that $p \sim L^{-3}$ [15]. Here we carry out a similar estimation for the kink-breather solution in the FK model and the result is shown in Fig. 6. The numerical data can be fitted as $p \sim L^{-3.5}$. There is evidence that for sufficiently small frequency of the breather the kink-breather system in the FK model with a small h^2 never splits [13].

All the important features of the KB fractal scattering

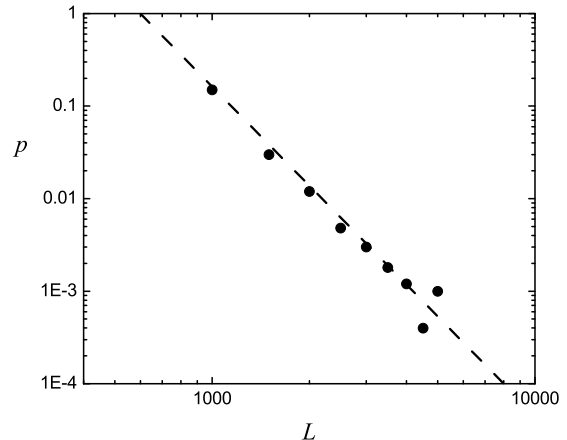


FIG. 6: Probability p to observe the kink-breather system with the lifetime L (in Fig. 5 we have $L \approx 55$). Numerical data is shown by dots and only the cases with $L > 1000$ were taken into account. Dashed line is the guide for an eye and it has slope -3.5.

including the existence of the two qualitatively different stochastic regions in the fractal structure will be clarified in Sec. III with the help of the three-particle model.

III. THREE-PARTICLE MODEL

A. Description of the model

Attempting to explain the effects observed in the three-soliton collisions in weakly perturbed SGE reported in Sec. II, we consider the solitary waves as effective particles, and study the dynamics of three such particles in one-dimensional space. The particles have mass $m = 8$, which is the rest mass of SGE kink, and they carry topological charges $q_j = \pm 1$. Particles with $q_j = 1$ ($q_j = -1$) will be called kinks (respectively, antikinks) by analogy with the SGE solitons. We assume that particles i and j , having coordinates x_i and x_j , interact via the potential

$$U_{ij}(r_{ij}) = 16 + q_i q_j \frac{16}{\cosh(r_{ij})}, \quad r_{ij} = x_j - x_i, \quad (6)$$

which qualitatively approximates the interaction of two SGE kinks. The potential of Eq. (6) is attractive for $q_i \neq q_j$ and repulsive for $q_i = q_j$. The binding energy of the kink-antikink pair is equal to 16, which is the energy of two standing SGE kinks. Note that for the kink and antikink at any finite distance r_{ij} the potential energy $U_{ij}(r_{ij})$ is less than 16. If the kinetic energy of relative motion of the particles is less than $16 - U_{ij}(r_{ij})$, then the particles cannot escape the mutual attraction and they form an oscillatory bound state, i.e., a breather.

The Hamiltonian of the three-particle system is

$$H = \frac{m}{2} \sum_{j=1}^3 v_j^2 + U_{12}(r_{12}) + U_{13}(r_{13}) + U_{23}(r_{23}), \quad (7)$$

where $v_j = dx_j/dt$, and there is one more integral of motion, namely the conservation of momentum. Without loss of generality, we assume that the total momentum in the system is equal to zero, i.e., $m(v_1 + v_2 + v_3) = 0$. Introducing new variables

$$x_2 - x_1 \rightarrow \sqrt{3}\alpha + \beta, \quad x_3 - x_1 \rightarrow 2\beta, \quad t \rightarrow \sqrt{2mt}, \quad (8)$$

the Hamiltonian of Eq. (7) can be presented in the form

$$H = \frac{1}{2} (\dot{\alpha}^2 + \dot{\beta}^2) + U_{12}(\sqrt{3}\alpha + \beta) + U_{13}(2\beta) + U_{23}(\sqrt{3}\alpha - \beta), \quad (9)$$

which is the Hamiltonian of a unit-mass particle moving in the two-dimensional scattering potential.

Now we solve numerically three equations of motion which can be derived from the Hamiltonian Eq. (7) and, inverting Eq. (8), present the three-particle dynamics by the trajectory of the particle in the (α, β) -plane.

B. Separatrix three-soliton solutions to SGE

Several separatrix three-soliton solutions to the exactly integrable SGE Eq. (3) have been reported in [12]. Here we reproduce two solutions important for our study.

The separatrix $K\bar{K}K$ solution is

$$\begin{aligned} u_{K\bar{K}K}(x, t) &= 4 \arctan(\exp x) + 4 \arctan \frac{R}{S}, \\ R &= \delta (\sinh F - \cosh G \sinh x), \\ S &= \delta (\cosh G + \sinh F \sinh x) - \cosh F \cosh x, \\ F &= -\delta x, \quad G = \delta Vt, \quad \delta^{-1} = \sqrt{1 - V^2}. \end{aligned} \quad (10)$$

In this highly symmetric solution the anti-kink is at rest and it is located at the point of collision of two kinks moving with the velocities V and $-V$.

The kink-breather separatrix solution is

$$\begin{aligned} u_{KB}(x, t) &= 4 \arctan(\exp x) + 4 \arctan \frac{X}{Y}, \\ X &= \eta (\sinh D - \cos C \sinh x), \\ Y &= \eta (\cos C + \sinh D \sinh x) - \cosh D \cosh x, \\ C &= -\omega t, \quad D = \eta x, \quad \eta = \sqrt{1 - \omega^2}, \end{aligned} \quad (11)$$

and it has only one parameter ω because it is a particular form of the KB solution where the kink and the breather have zero velocities and zero distance between them.

In Fig. 7 we plot (a) the SGE solution Eq. (10) for $V = 0.2$, (b) the three-particle dynamics in the (x, t) space for $q_1 = -q_2 = q_3 = 1$, $(v_0)_1 = -(v_0)_3$, $(v_0)_2 = 0$, $(x_0)_1 =$

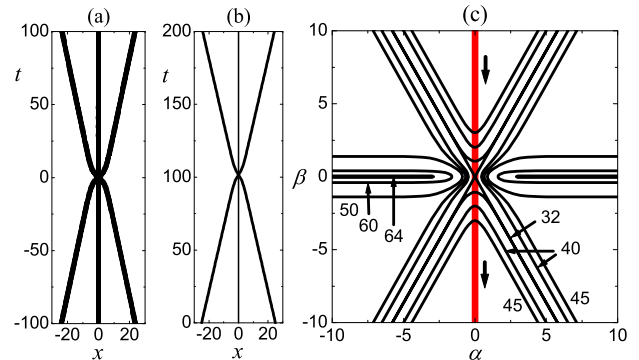


FIG. 7: (Color online) (a) The SGE solution of Eq. (10) for $V = 0.2$; (b) the three-particle dynamics with $q_1 = -q_2 = q_3 = 1$, $(v_0)_1 = -(v_0)_3$, $(v_0)_2 = 0$, $(x_0)_1 = -(x_0)_3 = -25$, and $(x_0)_2 = 0$ in the (x, t) space; (c) the red line shows the corresponding trajectory of the particle in the scattering potential in the (α, β) -plane (isopotential lines are shown in black). The particle in (c) moves along the potential ridge and this motion is unstable. The picture in (c) gives a visual image of the separatrix $K\bar{K}K$ solution Eq. (10).

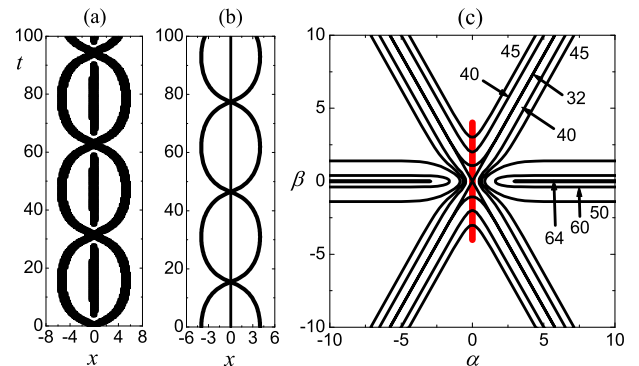


FIG. 8: (Color online) (a) The SGE solution Eq. (11) for $\omega = 0.2$; (b) the three-particle dynamics with $q_1 = -q_2 = q_3 = 1$, $(v_0)_1 = (v_0)_2 = (v_0)_3 = 0$, $(x_0)_1 = -(x_0)_3 = -4$, and $(x_0)_2 = 0$ in the (x, t) space; (c) the red line shows the corresponding trajectory of the particle in the scattering potential in the (α, β) -plane (isopotential lines are shown in black). The particle in (c) oscillates along the potential ridge and this motion is unstable. The picture in (c) gives a visual image of the separatrix KB solution Eq. (11).

$-(x_0)_3 = -25$, and $(x_0)_2 = 0$, and in (c) the red line shows the corresponding dynamics in the (α, β) -plane. In (c) the isolines of the scattering potential are also shown (black lines). The scattering potential in this case is a superposition of a ridge along $\beta = 0$ and two troughs along the lines $\beta = \pm\sqrt{3}\alpha$. Note that the intersection of

the ridge and the two troughs forms in the vicinity of the origin the ridge along the line $\alpha = 0$; the trajectory of the particle shown by the red line goes exactly on the top of this ridge. Obviously, this type of motion is unstable and, as we will see in the following, small variation in the initial conditions may result in qualitatively different dynamics of the particle. The picture presented in Fig. 7 (c) gives a visual image of the separatrix $K\bar{K}K$ solution Eq. (10).

In Fig. 8 we plot (a) the SGE solution Eq. (11) for $\omega = 0.2$, (b) the three-particle dynamics in the (x, t) space for $q_1 = -q_2 = q_3 = 1$, $(v_0)_1 = (v_0)_2 = (v_0)_3 = 0$, $(x_0)_1 = -(x_0)_3 = -4$, and $(x_0)_2 = 0$, and in (c) the red line shows the corresponding trajectory in the (α, β) -plane. The particle in (c) oscillates along the potential ridge and, similarly to the previous example, this motion is unstable. The picture presented in Fig. 8 (c) gives a visual image of the separatrix KB solution of Eq. (11).

When the red line passes the origin of the (α, β) -plane, from Eq. (8) one has $x_1 = x_2 = x_3$, i.e., all three particles meet at one point. In the SGE this corresponds to simultaneous collision of all three kinks.

Looking at Fig. 8(c) one can expect the possibility of oscillation of the particle along the ridge of the scattering potential with $\beta = 0$. This is indeed possible for the three-particle system but, from $\beta = 0$ one finds from Eq. 8 that $x_1(t) \equiv x_3(t)$, which cannot be realized in the FK model because the kinks have finite width.

C. Three-kink collisions

In Fig. 9 we compare the KKK and $KK\bar{K}$ symmetric collisions in the three-particle model for $(x_0)_1 = -(x_0)_3 = -25$, $(x_0)_2 = 0$ and $(v_0)_1 = -(v_0)_3 = 0.6$, $(v_0)_2 = 0$. The top panels show the three-particle dynamics in the (x, t) space. For each case, the bottom panels correspondingly show the equipotential lines of the scattering potential of Eq. (9) (black) and the trajectory of the particle (red line) in the (α, β) -plane. In (a') the scattering potential for $q_1 = q_2 = q_3 = 1$ is a superposition of three troughs while in (b') for $q_1 = q_2 = -q_3 = 1$ it is a superposition of a ridge and two troughs. The potential in Fig. 9 (b') can be obtained from that shown in Fig. 7 (c) and Fig. 8 (c) through a rotation by $-\pi/3$.

In Fig. 9 (a), the like particles repel each other and, in (a'), the particle hits the potential barrier and goes back. In (b), one can see that particles collide in two successive two-soliton collisions. In this case, the particle in (b') passes the two potential troughs one after another and then moves away from the origin in the direction symmetrically equivalent to the direction it came from. Since the red line in (a') and (b') never goes through the origin, the three particles never meet at one point.

In Fig. 10 we give two examples of near-separatrix $K\bar{K}K$ symmetric collisions in the three-particle model for $(x_0)_1 = -(x_0)_3 = -25$ and $(v_0)_1 = -(v_0)_3 = 0.6$, $(v_0)_2 = 0$. Recall that the separatrix solution shown in

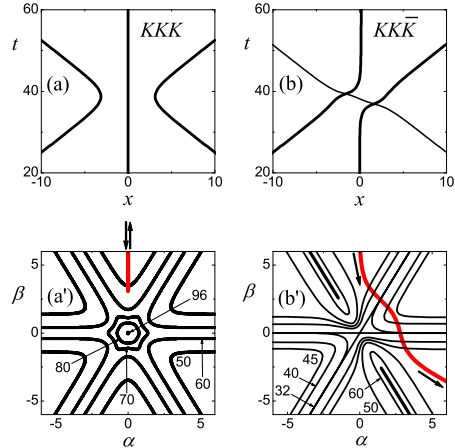


FIG. 9: (Color online) Comparison of (a,a') KKK and (b,b') $KK\bar{K}$ symmetric collisions. The top panels show the three-particle dynamics in the (x, t) space. The trajectories of kinks are shown by thicker lines than those of antikinks. The bottom panels correspondingly show the equipotential lines of the scattering potential Eq. (9) (black) and the trajectory of particle (red line) in the (α, β) -plane. The parameters are $(x_0)_1 = -(x_0)_3 = -25$, $(x_0)_2 = 0$ and $(v_0)_1 = -(v_0)_3 = 0.6$, $(v_0)_2 = 0$. The charges of the particles are (a,a') $q_1 = q_2 = q_3 = 1$ and (b,b') $q_1 = q_2 = -q_3 = 1$.

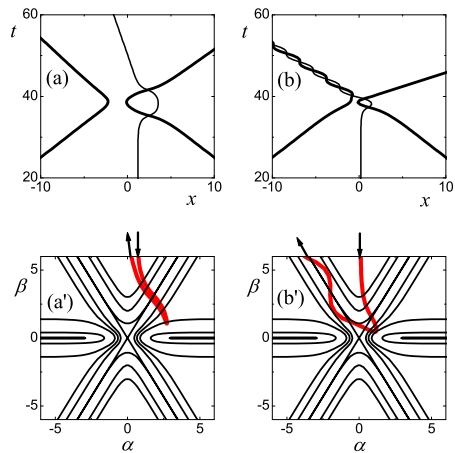


FIG. 10: (Color online) Sensitivity of the result of near separatrix collision to a small deviation from $(x_0)_2 = 0$ demonstrated by setting (a,a') $(x_0)_2 = 1.2$ and (b,b') $(x_0)_2 = 0.2$. In (a,a') only a quantitative change in the system can be seen upon collision [compare with the actual three-kink collision in FK model shown in Fig. 2(a')]. In (b,b'), kink and antikink merge in a breather [compare with Fig. 2(b')]. Other parameters: $(x_0)_1 = -(x_0)_3 = -25$ and $(v_0)_1 = -(v_0)_3 = 0.6$, $(v_0)_2 = 0$.

Fig. 7 corresponds to $(x_0)_2 = 0$ but Fig. 10 corresponds to (a,a') $(x_0)_2 = 1.2$ and (b,b') $(x_0)_2 = 0.2$. In Fig. 10 (a,a'), the deviation from the separatrix is rather large and only quantitative changes in the particle parameters can be seen. This should be compared with the actual three-kink collision in FK model shown in Fig. 2(a'). In (b,b'), kink and antikink merge in a breather [compare with Fig. 2(b')]. Taking into account the time reversibility in the Hamiltonian systems, this picture can be also regarded as an illustration of the breakup of a breather colliding with a kink.

The three-particle model explains why the REE effect is more pronounced for the solitons colliding with a small relative velocity. For the particle moving in the (α, β) -plane along the separatrix [red line in Fig. 7(c)], any perturbation results in exponential in time deviation from the potential ridge. High-speed collision results in faster passing of the scattering potential and the trajectory of the particle cannot be considerably changed. The situation is opposite for the slow particle, which corresponds to the collision of solitons with a small relative velocity.

D. Kink-breather collisions

Here we select the parameters of the three particles so as to simulate the collisions between a kink and a breather. In particular, we set the charges of particles as $q_1 = -q_2 = q_3 = 1$, their initial velocities as $(v_0)_1 = (v_0)_2 = 0.3$, $(v_0)_3 = -0.6$; the initial positions of the particles constituting the "breather" are $(x_0)_1 = -16$, $(x_0)_2 = -13.5$, and the third particle initial position was varied. In Fig. 11 the results are shown for (a) $(x_0)_3 = 30.51$, (b) $(x_0)_3 = 23.398$, and (c) $(x_0)_3 = 23.391$. The top panels show the three-particle dynamics in the (x, t) space, while the bottom panels show the corresponding trajectory of the particle in the (α, β) -plane (red line).

Collisions in (a) and (b) are elastic but the difference is that while in (a') the particle does not move along the separatrix line $\alpha = 0$, in (b') it does, and a very small change in the initial conditions is sufficient to have a qualitatively different result of the collision, as presented in (c),(c'), where the breather reflects from the kink [compare (c) with actual kink-breather collision in the FK model shown in Fig. 3(b')].

E. Fractal kink-breather scattering

To reproduce the kink-breather fractal scattering described in Sec. II B for the FK model we set the following parameters for the particles in the three-particle model: $q_1 = -q_2 = q_3 = 1$, $(v_0)_1 = (v_0)_2 = (v_0)_3 = 0$, $(x_0)_1 = -(x_3)_2 = -5$, and variable $(x_0)_2$.

In Fig. 12 we present the velocities of particles after collision \tilde{v}_j as the function of $(x_0)_2$. In (b) a blowup of the self-similar region indicated in (a) is presented. Comparison of the panels (a) and (b) with the corresponding

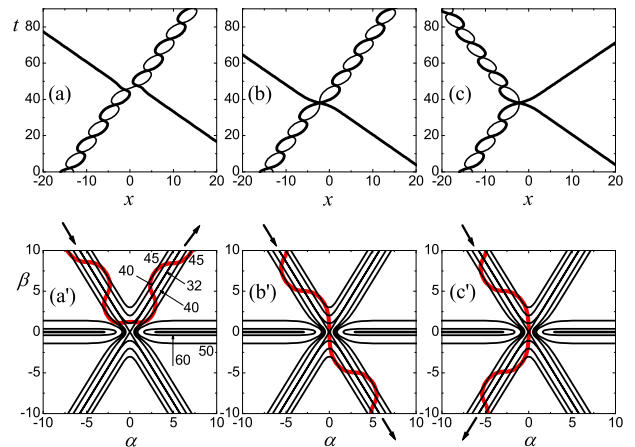


FIG. 11: (Color online) Three-particle model simulating the kink-breather collisions. The top panels show the three-particle dynamics in the (x, t) space, while the bottom panels show the corresponding trajectory of the particle in the (α, β) -plane (red line). Only the initial position of the third particle is varied: (a) $(x_0)_3 = 30.51$, (b) $(x_0)_3 = 23.398$, and (c) $(x_0)_3 = 23.391$. Collisions in (a),(a') and (b),(b') are elastic but in the latter case it is close to the separatrix (see Fig. 8) resulting in a great sensitivity to variations in initial conditions, as demonstrated in (c),(c'). The rest of the parameters are chosen as $q_1 = -q_2 = q_3 = 1$, $(v_0)_1 = (v_0)_2 = 0.3$, $(v_0)_3 = -0.6$, $(x_0)_1 = -16$, $(x_0)_2 = -13.5$.

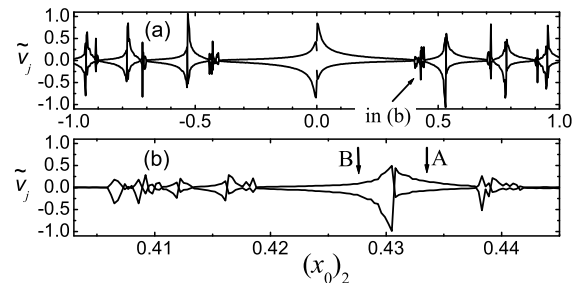


FIG. 12: Fractal three-particle scattering. Panels (a) and (b) should be compared with the corresponding panels of Fig. 4. Parameters: $q_1 = -q_2 = q_3 = 1$, $(v_0)_1 = (v_0)_2 = (v_0)_3 = 0$, $(x_0)_1 = -(x_3)_2 = -5$, and variable $(x_0)_2$.

panels of Fig. 4 reveals the qualitative similarity in the KB collision outcome in the FK model and in the three-particle model. We note that while we expect this particle model to bear the essential qualitative characteristics of the three-particle collisions, their details depend sensitively on the precise initial conditions; for this reason, we expect Fig. 12 to match *qualitatively* the results of Fig. 4.

One of the important elements of the usefulness of the

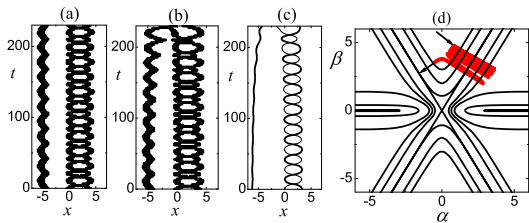


FIG. 13: (Color online) (a) The exact KB solution to the SGE, (b) the same solution in the weakly discrete FK model, (c) the three-particle dynamics in the (x, t) space and (d) the corresponding dynamics in the (α, β) space. In (a), (b), kink and breather have zero initial velocities, breather frequency is $\omega = 0.3$, and separation between the kink and the breather is equal to 1.2. In (c), (d), $q_1 = -q_2 = q_3 = 1$, $(v_0)_1 = (v_0)_2 = (v_0)_3 = 0$, $(x_0)_1 = -6.18$, $(x_0)_2 = 0$, $(x_0)_3 = 3.3$.

three-particle model is that it gives the possibility to analyze the KB fractal scattering from a different point of view, namely, by looking at the corresponding dynamics of the particle in the scattering potential in the (α, β) space. In Fig. 13 we show (a) the exact KB solution to the SGE, (b) the same solution in the weakly discrete FK model, (c) the three-particle dynamics in the (x, t) space and (d) the corresponding dynamics in the (α, β) space. In (a), (b), kink and breather have zero initial velocities, breather frequency is $\omega = 0.3$, and separation between the kink and the breather is equal to 1.2 (we refer to the form of the KB solution given in [12]). In (c), (d), $q_1 = -q_2 = q_3 = 1$, $(v_0)_1 = (v_0)_2 = (v_0)_3 = 0$, $(x_0)_1 = -6.18$, $(x_0)_2 = 0$, $(x_0)_3 = 3.3$. One can see from Fig. 13 that the distance between the kink and the breather does not change in time in the integrable system [shown in (a)] but in the nonintegrable ones the distance between them gradually decreases and they eventually collide [see (b) and (c)]. The separated kink and breather having zero velocities are presented in the (α, β) space by the particle oscillating along the line normal to the trough with orientation $\beta = \sqrt{3}\alpha$ (kink is to the left of the breather) or $\beta = -\sqrt{3}\alpha$ (kink is to the right of the breather). However, the troughs have a slope toward the origin of the (α, β) plane and the oscillating particle gradually approaches the origin, i.e., the collision point of three particles. After the particle has approached the origin [this situation is shown in Fig. 13 (d)], two qualitatively different scenarios giving different fractal patterns are possible.

The *first scenario* is shown in Fig. 14. Here the particle after making a few oscillations normally to the trough $\beta = \sqrt{3}\alpha$ can cross the separatrix line $\alpha = 0$ and make a few oscillations normally to the trough $\beta = -\sqrt{3}\alpha$ and then again cross the separatrix line changing the trough. While the particle performs such crossings of the separatrix it remains close to the origin of the (α, β) plane

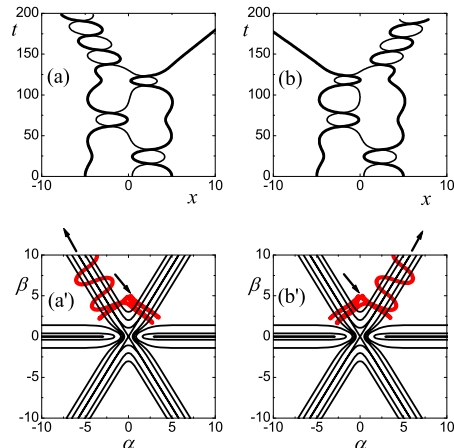


FIG. 14: (Color online) Illustration of one of the two possible scenarios of fractal kink-breather scattering. (a),(b) show the dynamics of three particles in the (x, t) plane while (a'),(b') the corresponding dynamics in the (α, β) plane. The particle in (a'),(b') after making a few oscillations normally to the trough $\beta = \sqrt{3}\alpha$ can cross the separatrix line $\alpha = 0$ and make a few oscillations normally to the trough $\beta = -\sqrt{3}\alpha$ and then again cross the separatrix line changing the trough. While the particle performs such crossings of the separatrix it remains close to the origin and thus, all three particles are close to each other. This defines the lifetime of the multi-soliton bound state discussed in [14, 15, 24]. Eventually, the particle will move away from the origin along one of the troughs. Parameters: $(v_0)_i = 0$, $i = 1, 2, 3$, $(x_0)_1 = -(x_0)_3 = -5$, (a) $(x_0)_2 = 0.433$ and (b) $(x_0)_2 = 0.4275$.

and thus, all three particles are close to each other. This defines the lifetime of the multi-soliton bound state discussed in [14, 15, 24]. The probability to have a three-particle bound state with a long lifetime is small (see Fig. 6) meaning that eventually the particle will move away from the origin along one of the troughs remaining in the half-plane $\beta > 0$ (compare Fig. 14 with Fig. 5 where the KB dynamics in the FK model is presented).

The *second scenario* is more obvious because it is directly related to the separatrix solution Eq. (11) presented in Fig. 8. After making a few oscillations normally to the trough $\beta = \sqrt{3}\alpha$ as shown in Fig. 13 (d), the particle can be sent by the scattering potential almost exactly along the separatrix line $\alpha = 0$. Then the particle will make several oscillations along the ridge of the potential, as shown in Fig. 8 (c), before the inherent instability of this trajectory “ejects” the particle away from the origin in one of the four directions along the troughs $\beta = \pm\sqrt{3}\alpha$. This contrast to the first scenario where the particle can be scattered by the potential in the two of the four directions, namely, in the ones with $\beta > 0$.

The first scenario is associated with the self-similar regions connecting the two “butterflies” [see Fig. 4 (b)

and (c)] while the second one is associated with the self-similar regions connecting the “wings” of a “butterfly” [see Fig. 4 (d)]. However, the whole fractal pattern is the result of the combination of both mechanisms. Each scenario is related to a periodic orbit of the particle in the scattering potential [28]. In the second scenario the periodic orbit is the separatrix kink-breather solution shown in Fig. 8, while in the first scenario there exists an infinite set of periodic orbits. One particular orbit can be described as follows: the particle in the scattering potential makes N oscillations almost normally to the trough $\beta = \sqrt{3}\alpha$ and then jumps to the trough $\beta = -\sqrt{3}\alpha$ where it also makes N oscillations and then returns to the trough $\beta = \sqrt{3}\alpha$ completing one period of the periodic orbit [Fig. 14 (a') and (b')] give examples when the particle makes such jumps between the troughs $\beta = \pm\sqrt{3}\alpha$ but in these cases the trajectories are aperiodic]. If the particle follows a periodic orbit exactly, the three-particle system never experiences a breakup; however, the eventual separation of the structures is a result of the dynamical instability of such periodic orbits.

It is well-known that the probability p of the time delay T for the particle interacting with the scattering potential *without* the periodic orbits decreases exponentially with T while in the presence of the periodic orbits it decreases algebraically [28]. The scattering potential in our case does have the periodic orbits and the probability p to observe a bound state with the lifetime L (analogous to the time delay T) decreases algebraically, $p \sim L^{-\alpha}$. This was found in [15] for the two-soliton collisions in the weakly perturbed NLSE, and in the present study this was also confirmed for the kink-breather system in the FK model, as presented in Fig. 6.

IV. DISCUSSION AND CONCLUSIONS

Through direct numerical simulations, we have presented some of the striking effects generated by even a weak breaking of integrability (via discretization) in the sine-Gordon model. We have indicated that alternative mechanisms such as the excitation of internal modes and the emission of phonon radiation are too weak to explain the phenomena observed in numerical simulations, and we have therefore attributed them to the radiationless energy exchange between the solitons. Indeed, these effects have been systematically explained in a qualitative fashion in the framework of the three-particle model suggested in Sec. III A, lending direct support to the conclusion that all the nontrivial effects are due to the *radiationless energy exchange* between colliding solitons [2, 9, 10, 11, 12, 13, 14, 15, 16, 17]. The following is known about the REE effects: (i) Manifestations of the REE effect grow proportionally to the perturbation parameter ϵ while radiation and excitation of soliton internal modes grow as ϵ^2 . (ii) In the sine-Gordon model the REE effect can happen only if at least three solitons collide simultaneously. Energy exchange in the two-soliton

collision is suppressed by the two conservation laws that remain exactly or approximately preserved in the weakly perturbed system. (iii) The REE effect is related to the existence of the separatrix multi-soliton solutions to the integrable equations. Near-separatrix motion is extremely sensitive to the perturbations [29]. (iv) The REE effect can be responsible for the fractal soliton scattering.

The REE effect is generic and some of the above conclusions can be also extended to other nearly integrable models [2]. For instance, the REE effect is observed in the weakly perturbed NLSE already in two-soliton collisions because here each soliton has two parameters and the total number of parameters describing the two-soliton solution (four) exceeds the number of the remaining conservation laws. On the other hand, the REE is *not* possible in the weakly perturbed KdV equation or weakly perturbed Toda lattice [30] because in these cases the soliton's cores never merge during collisions and thus, the multi-particle effects are absent. Interestingly, the fractal pattern of different nature (not related to REE) is possible in KdV systems [31].

The three-particle model offered in the present study can be reduced to the study of the dynamics of a particle interacting with the two-dimensional scattering potential. Such a reduction gives a clear interpretation of the abovementioned features of the REE effect observed in the three-soliton collisions. Particularly, the following features have been identified:

1. The three-particle model gives a visual image of the separatrix three-kink and kink-breather solutions to the integrable SGE, see Fig. 7 and Fig. 8. The separatrix solution corresponds to motion of the particle along a ridge of the scattering potential.
2. KKK collisions and $KK\bar{K}$ collisions are always practically elastic while $K\bar{K}K$ collisions are strongly inelastic in the vicinity of $(x_0)_2$. Only in the latter case the point moves along the ridge of the scattering potential, which is the motion along a separatrix, see Fig. 7. Also only in $K\bar{K}K$ collisions the point passes through the origin of the scattering potential which means that the three kinks collide at one point simultaneously.
3. The three-particle model explains why the REE effect is more pronounced for the solitons colliding with a small relative velocity. For the particle moving in the (α, β) -plane along the separatrix [red line in Fig. 7(c)], any perturbation results in exponential in time deviation from the potential ridge. High-speed collision results in faster passing of the scattering potential and the trajectory of the particle cannot be considerably changed. The situation is opposite for the slow particle, which corresponds to the collision of solitons with a small relative velocity.
4. The fractal soliton scattering is explained by the presence of the periodic orbits of the particle in the

scattering potential. Periodic orbits of two types were found, each of them is responsible for a particular scenario of the particle dynamics, and each scenario yields a self-similar pattern for the collision outcome as a function of a parameter, such as the location of the central effective particle (Sec. III E).

5. Periodic orbits are also responsible for the algebraic law $p \sim L^{-\alpha}$, where p is the probability to observe the three-soliton bound state with the lifetime L (see Fig. 6 and Sec. III E).

In the weakly perturbed systems the REE is the dominant effect. However, if the perturbation is not small, the energy exchange effect is mixed with radiation and possibly with excitation of internal modes. We thus believe that the net effect of inelasticity of soliton collisions

can be decomposed into three major parts: the radiationless energy exchange, excitation of the soliton's internal modes, and emission of radiation. This highlights the need for a systematic study as a function of increasing deviations from the integrable regime of the relative role of these three complementary mechanisms. Such a study would be of particular interest for future investigations.

Acknowledgments

The authors thank A.A. Sukhorukov for useful discussions. SVD acknowledges a financial support of the Russian Foundation for Basic Research, grant 07-08-12152. PGK acknowledges a support from NSF-DMS-0204585, NSF-DMS-0505663, NSF-CAREER, and the Alexander von Humboldt Foundation.

-
- [1] Yu.S. Kivshar and B.A. Malomed, *Rev. Mod. Phys.* **61**, 763 (1989).
 - [2] P.G. Kevrekidis and S.V. Dmitriev, *Soliton Collisions*, in *Encyclopedia of Nonlinear Science*, Edited by A. Scott (Routledge, New York, 2005), PP. 148-150.
 - [3] M.J. Ablowitz and H. Segur, *Solitons and the Inverse Scattering Transform*, SIAM (Philadelphia, 1981).
 - [4] Yu.S. Kivshar, D.E. Pelinovsky, T. Cretegny, and M. Peyrard, *Phys. Rev. Lett.* **80**, 5032 (1998).
 - [5] P. Anninos, S. Oliveira, and R.A. Matzner, *Phys. Rev. D* **44**, 1147 (1991).
 - [6] D. K. Campbell, J. F. Schonfeld, and C. A. Wingate, *Physica D* **9**, 1 (1983); M. Peyrard and D. K. Campbell, *Physica D* **9**, 33, (1983); D.K. Campbell and M. Peyrard, *Physica D* **18**, 47 (1986); *ibid.* **19**, 165 (1986).
 - [7] T. I. Belova and A. E. Kudryavtsev, *Phys. Usp.* **40**, 359 (1997).
 - [8] R.H. Goodman and R. Haberman, *SIAM J. Appl. Dyn. Sys.* **4**, 1195 (2005); R.H. Goodman and R. Haberman, *Phys. Rev. Lett.* **98**, 104103 (2007).
 - [9] S.V. Dmitriev, L.V. Nauman, A.A. Ovcharov, and M.D. Starostenkov, *Russian Physics Journal* **39**, 164 (1996).
 - [10] H. Frauenkron, Yu.S. Kivshar, and B.A. Malomed, *Phys. Rev. E* **54**, R2244 (1996).
 - [11] S.V. Dmitriev, L.V. Nauman, A.M. Wusatowska-Sarnek, and M.D. Starostenkov, *phys. stat. sol. (b)* **201**, 89 (1997).
 - [12] A. E. Miroshnichenko, S. V. Dmitriev, A. A. Vasiliev, and T. Shigenari, *Nonlinearity* **13**, 837 (2000).
 - [13] S.V. Dmitriev, T. Miyauchi, K. Abe, and T. Shigenari, *Phys. Rev. E* **61**, 5880 (2000).
 - [14] S.V. Dmitriev, Yu.S. Kivshar, and T. Shigenari, *Phys. Rev. E* **64**, 056613 (2001).
 - [15] S. V. Dmitriev and T. Shigenari, *Chaos* **12**, 324 (2002).
 - [16] S. V. Dmitriev, D. A. Semagin, A. A. Sukhorukov, and T. Shigenari, *Phys. Rev. E* **66**, 046609 (2002).
 - [17] S. V. Dmitriev, P.G. Kevrekidis, B.A. Malomed, and D.J. Frantzeskakis, *Phys. Rev. E* **68**, 056603 (2003).
 - [18] J. A. Combs and S. Yip, *Phys. Rev. B* **28**, 6873 (1983).
 - [19] R. Boesch, C. R. Willis, and M. El-Batanouny, *Phys. Rev. B* **40**, 2284 (1989).
 - [20] R. Boesch and M. Peyrard, *Phys. Rev. B* **43**, 8491 (1991).
 - [21] Y. Ishimori and T. Munakata, *J. Phys. Soc. Jpn.* **51**, 3367 (1982).
 - [22] J. Yang and Y. Tan, *Phys. Rev. Lett.* **85**, 3624 (2000).
 - [23] Y. Tan and J. Yang, *Phys. Rev. E* **64**, 056616 (2001).
 - [24] Y. Zhu, R. Haberman, and J. Yang, *Phys. Rev. Lett.* **100**, 143901 (2008); Y. Zhu and J. Yang, *Phys. Rev. E* **75**, 036605 (2007).
 - [25] V.I. Karpman and V.V. Solov'ev, *Physica D* **3**, 142 (1981).
 - [26] I.E. Papacharalampous, P.G. Kevrekidis, B.A. Malomed, and D.J. Frantzeskakis, *Phys. Rev. E* **68**, 046604 (2003).
 - [27] R. Hirota, *J. Phys. Soc. Jpn.* **33**, 1459 (1972).
 - [28] E. Ott and T. Tel, *Chaos* **3**, 417 (1993).
 - [29] G. M. Zaslavsky, R. Z. Sagdeev, D. A. Usikov, and A. A. Chernikov *Weak Chaos and Quasi-Regular Patterns* (Cambridge Univ. Press, Cambridge, 1991).
 - [30] M. Toda, *Theory of Nonlinear Lattices*, Springer-Verlag (New York, 1989).
 - [31] E. Zamora-Sillero and A.V. Shapovalov, *Phys. Rev. E* **76**, 046612 (2007).